Rapid, modular biosynthesis of plant hemicellulose and its impact on yeast cells

Running title: Domain swapping of (gluco)mannan synthases

Madalen Robert[1], Julian Waldhauer[1], Fabian Stritt[2], Bo Yang[1], Markus Pauly[2], Cătălin Voiniciuc[1,*]

[1] Independent Junior Research Group–Designer Glycans, Leibniz Institute of Plant Biochemistry, 06120 Halle (Saale), Germany

[2] Institute for Plant Cell Biology and Biotechnology, Heinrich Heine University, Düsseldorf, Germany

*For correspondence (email: catalin.voiniciuc@ipb-halle.de).

SUMMARY

Interest in the engineering of polysaccharide-based biomaterials has emerged in recent years. Despite impressive advances on bacterial cellulose, comparatively little is known about how plant hemicelluloses can be reconstituted and modulated in cells suitable for biotechnological purposes. Here, we optimized the cultivation of the yeast *Pichia pastoris* for the orthogonal production of plant polysaccharides, and enhanced heteromannan (HM) production by assembling modular cellulose synthase-like A (CSLA) enzymes. Chimeric proteins swapping the domains of a plant mannan synthase and a glucomannan synthase led, in three cases, to higher yields or improved growth compared to the parental CSLA enzymes. Prolonged expression of a glucomannan synthase from *Amorphophallus konjac* (AkCSLA3) was toxic to yeast cells, as demonstrated by reduced biomass accumulation and elevated uptake of dyes that are normally restricted to the extracellular matrix. However, no growth inhibition was observed for CSLA variants producing relatively pure mannan or a CSLC glucan synthase. The toxicity of AkCSLA3 was reduced by swapping its C-terminal region with that of a mannan synthase. HM production was further boosted by co-expressing chimeric CSLA proteins with the MANNAN-SYNTHESIS-RELATED1 (MSR1) putative glycosyltransferase. Interestingly, *Pichia* cells either increased or decreased in size depending on the CSLA variant expressed, and most of them remained viable even producing copious amounts of hemicellulose. Therefore, yeast modified with non-toxic plant polysaccharides could represent a modular chassis to produce and protect sensitive cargo such as therapeutic proteins.

Keywords: cell wall biosynthesis, hemicellulose, glycosyltransferase, chimeric enzymes, mannan, glucomannan, glucan, *Pichia pastoris,* synthetic biology

SIGNIFICANCE STATEMENT

Hemicelluloses encapsulate all plant cells and are valuable industrial biomaterials, but the production of tailor-made plant polysaccharides remains challenging. Using chimeric cellulose synthase-like enzymes in a modular yeast expression system, plant heteromannan were produced in large amounts and had tunable effects on cell growth and morphology.

INTRODUCTION

Enzymes from the cellulose synthase superfamily produce the most abundant polysaccharides on Earth, including cellulose and a variety of hemicelluloses. Greater interest in the engineering of polysaccharide-based biomaterials has emerged in recent years. Synthetic biology efforts in this area have been largely restricted to bacterial cellulose due to its well-characterized production (Gilbert and Ellis, 2019; Gilbert *et al.*, 2021). Although suitable orthogonal hosts have been identified (Pauly *et al.*, 2019), comparatively little is known about how the biosynthesis of plant hemicelluloses by glycosyltransferases (GTs) could be reconstituted and modulated in non-plant cell factories. GTs from the Cellulose Synthase-Like (CSL) superfamily produce the backbones of xyloglucans, heteromannans (HM), as well as β-1,3-1,4-linked-glucans (Pauly *et al.*, 2013; Scheller and Ulvskov, 2010), which can account for one-third or more of the cell wall biomass. Of these polymers, HMs appear to have the simplest structures since they can be found as linear β-1,4-linked mannans (defined as containing >90% mannose, Man), or as glucomannans that also contain β-1,4-linked glucose (Glc) units (Buckeridge, 2010). (Gluco)mannans can be decorated with galactose side chains (Voiniciuc *et al.*, 2015; Yu *et al.*, 2018) or *O*-acetylated (Zhong *et al.*, 2018; Zhong *et al.*, 2019), which increases their solubility (Berglund *et al.*, 2020). HM is abundant in the endosperms of most legume seeds (Bewley *et al.*, 2013), and to a lesser extent in cereal grains (Verhertbruggen *et al.*, 2021). Plant HM polymers confer important physiological properties, such as stabilizing extracellular matrices, which are also commercially valuable (Bewley *et al.*, 2013). For example, locust bean gum (extracted from *Ceratonia siliqua*, also known as carob) and guar gum (from *Cyamopsis tetragonoloba*) are commonly used hydrocolloids in the food (approved as E410 and E412 stabilizers within the European Union), cosmetic and pharmaceutical industries.

HM backbones are elongated in the Golgi apparatus by CSL clade A (CSLA) enzymes from GDP-Man and GDP-Glc precursors. CSLAs are expected to function together with GT34 enzymes and/or *O*-acetyltransferases to produce branched hemicelluloses, in order to avoid intracellular self-aggregation in the Golgi and thus facilitate their secretion to the extracellular matrix (Scheller and Ulvskov, 2010). Despite resembling CSLAs, CSL family C (CSLC) proteins required for xyloglucan synthesis (Kim *et al.*, 2020) have distinct numbers of transmembrane domains, which can lead to opposite topologies at the Golgi membrane (Davis *et al.*, 2010). Recently, HM biosynthesis was reconstituted in the yeast *Pichia pastoris* (also known as *Komagataella phaffi*) by the expression of CSLA enzymes with or without MANNAN-SYNTHESIS-RELATED (MSR) co-factors (Voiniciuc *et al.*, 2019). The biochemical activity of MSR putative GTs remains to be shown, but they likely modulate (gluco)mannan elongation by interacting with CSLA enzymes or post-translationally modifying them. The distinct HM structures found in plant tissues could be generated by GT specificity and/or sugar substrate availability. There is increasing evidence for the former hypothesis, since the *Amorphphallus konjac* AkCSLA3 produced glucomannan in yeast cells, while the expression of *Arabidopsis thaliana* AtCSLA2 alone only led to the accumulation of pure mannan (Voiniciuc *et al.*, 2019). Even though AtCSLA2 participates in galactoglucomannan elongation for Arabidopsis seed mucilage (Yu *et al.*, 2014; Voiniciuc *et al.*, 2015), the enzyme alone has a low preference for Glc incorporation *in vitro*

(Liepman *et al.*, 2005) or in living yeast cells without the co-expression of the AtMSR1 protein co-factor (Voiniciuc *et al.*, 2019).

To date, no study has looked specifically at how CSLA protein motifs influence (gluco)mannan biosynthesis. Domain swap experiments can provide insight into the structures and functions of related enzymes. Previously, two studies reported domain swap experiments for CSLF proteins involved in mixed-linkage glucan synthesis (Jobling, 2015; Dimitroff *et al.*, 2016). The expression of chimeric CSLF6 enzymes from several monocot species in *Nicotiana benthamiana* leaves revealed protein regions that modulate β-1,3-1,4-linked-glucan structure. Tailoring the production of hemicelluloses could lead to the engineering of grains enriched in fibers that are beneficial to human health (Collins *et al.*, 2010), or could be applied to engineer living materials (Gilbert and Ellis, 2019).

The aim of our study was to modulate the production of plant HM in a biotechnologically important yeast and to decipher how this impacts the engineered cells (Figure 1a), which could provide a valuable chassis for future biomaterial and therapeutic applications. We optimized the cultivation of *Pichia pastoris* for orthogonal production of plant hemicellulosic polysaccharides, and enhanced HM production by assembling modular, chimeric CSLA enzymes. *Pichia* cells were promising hosts to study CSLC and CSLA activities (Cocuron *et al.*, 2007; Gille *et al.*, 2011; Voiniciuc *et al.*, 2019; Pauly *et al.*, 2019), but the impact of the plant polymers was not previously investigated. Here, we extend their utility by improving the speed of modular enzyme expression and the hemicellulose yields. Prolonged expression of the AkCSLA3 glucomannan synthase was toxic to yeast cells, but this impairment was restored by swapping its C-terminal region with that of AtCSLA2. Two additional chimeric CSLAs enzymes enhanced plant mannan production compared to the native AtCSLA2 enzyme with minimal impact on growth and morphology. This synthetic biology strategy could also be applied to other CSL enzymes to synthesize additional biomaterials.

RESULTS

Modular Engineering of Cellulose Synthase-Like Enzymes and Cell Walls

To create chimeric CSLA proteins that modulate (gluco)mannan production, we first compared AkCSLA3 and AtCSLA2 sequences. TOPCONS (Tsirigos *et al.*, 2015), which integrates multiple algorithms, predicts that both proteins have a consensus topology with five transmembrane domains and a catalytic site facing the cytosol (Figure 1b). We delimited the proteins into four regions sharing 38% to 73% amino acid similarity, demarcated by border regions that contain at least 6 identical residues (Figure 1b). The second region contains most of the conserved GT2 domain (Pfam PF13641), which is involved in transferring glycosyl residues. Following sequence domestication of AkCSLA3 and AtCSLA2 to remove unwanted type IIS recognition sites (Table S1), we amplified and assembled chimeric CSLAs sequences using the GoldenPiCs toolkit (Figure 1c) that contains many modular parts for *Pichia* expression (Prielhofer *et al.*, 2017). Reciprocal chimeric constructs were created for each (gluco)mannan synthase, each containing one swapped domain from AtCSLA2 or AkCSLA3 (Figure 1d). The chimeric constructs were labelled according to the origin of the four domains (e.g. 2322 contains the second domain of AkCSLA3). The GoldenPiCs toolkit, which is

based on Golden Gate cloning (Engler *et al.*, 2008), enabled the seamless assembly of multiple CSLA fragments in the desired order, without introducing any mutations (Figure S1). Once the BB1 parts were verified, the coding sequences were assembled into a GoldenPiCs BB3 level vector together with the strong methanol (M) inducible promotor *pAOX1* and the *RPP1Btt* transcriptional terminator. Linearized transcriptional units were stably integrated in the *AOX1* region of the *Pichia* genome, and Zeocin-resistant colonies were verified by PCR to unambiguously confirm the chimeras (Figure S2).

To compare the engineered *CSLA* strains, we established a more efficient growth protocol compared to previous work, which required cells grown in buffered complex media to be washed or grown for 60 h prior to M induction (Cocuron *et al.*, 2007; Voiniciuc *et al.*, 2019). Reagent costs, hands-on steps, and incubation times were greatly reduced by cultivating cells in autoclavable 24 deep-well plates and YP-based media, containing yeast extract, peptone, and at least one carbon source. Most *Pichia* studies pre-culture cells in buffered media containing glycerol (G), an ideal carbon source for yeast biomass accumulation, but this must be washed out or depleted since it represses the *pAOX1* promoter. We found that *Pichia* AtCSLA2 and AkCSLA3 strains accumulated significant amounts of alkaline-insoluble (AKI) HM compared to the Venus fluorescent protein control when cells were grown directly in YPM for 48 h (Figure 2a). The amount of Man produced by CSLA strains was increased by an average of 60% by using YPM+G (Figure 2b), containing a limited amount of G to boost biomass accumulation. While we focused only on the top HM-producing colony for each chimeric CSLA variant (Figure 2), initial screening showed that independent transformants produced similar amounts of HM polymers based on AKI monosaccharide composition or β-mannanase digestion (Figure S3a). Since co-feeding a limited amount of G also yielded consistent biomass accumulation (Figure S3b), we selected the YPM+G medium for further structural evaluations of the polysaccharides synthesized by chimeric enzymes.

While the selected CSLA domains were similar in length and predicted topology (Figure 1), the swaps of individual regions had significant, unidirectional consequences on HM biosynthesis. Terminal domain swaps (3222 and 2223) for AtCSLA2, and N-terminal swap for AkCSLA3 (2333) resulted in a nearly complete loss of mannan production (Figure 2 and Figure S3), reminiscent of the reduction of CSLA activity associated with adding fluorescent tags (Voiniciuc *et al.*, 2019). Indeed, we resorted to analyzing untagged chimeric proteins, because AtCSLA2 lost its activity when we added N- or C-terminal fluorescent protein tags. Replacement of the second or third domain of AkCSLA3 (3233 and 3323) led to the production of intermediate levels of HM compared to the parental enzymes and the Venus negative control. While most of the domain swaps impaired hemicellulose synthesis, three of the chimeric enzymes (2322, 2232 and 3332) produced HM amounts that were up to 2-fold higher than the parental controls (Figure 2).

Glycosidic linkage analysis was performed to investigate the precise composition of AKI polymers made by the engineered CSLAs. All eight CSLA chimeric proteins produced significantly more 4-Man linkages compared to the Venus control (Figure 3), which only has trace amounts (less than 0.001% of total linkage area). The 4-linked Man represented 4–12% of linkages made by five of the chimeric CSLAs (Figure 3 and Table S2), which was significantly less than the amounts (27–40%) made by the parental enzymes and top three swaps (2322, 2232, and 3332). Despite the increases in

Man by all CSLA strains, only three constructs (AkCSLA3 glucomannan synthase, 2232 and 3332) showed significant increases in 4-Glc amounts relative to the Venus control (Figure 3), which contains small amounts of this linkage likely derived from glycogen (Pauly *et al.*, 2019). Glucomannan production by AkCSLA3 and 3332 was supported by both glycosidic linkage (Figure 3) and β-mannanase digestion analyses (Figure S3a). In contrast, the latter experiment did not support the ability of 2232 to produce glucomannan (Figure S3a). All CSLA variants made linear HMs polymers in yeast since the branched 4,6-Man units remained below 1% of linkage area (Table S2).

Influence of Top Domain Swaps on (Gluco)mannan Production

Since some of the generated swaps displayed reduced HM synthesis, only the top three most promising swaps (2322, 2232 and 3332) were chosen for further investigation and re-grown multiple times. The engineered yeast cell wall material was subjected to comprehensive analyses of HM polysaccharides (Figure 4 and Table S3). The release of carbohydrates containing both Glc and Man by endo-β-mannanase were only representative of the AkCSLA3 and 3332 *Pichia* strains (Figure 4a). In contrast, digestion of AtCSLA2, 2322 and 2232 proteins (containing regions of AkCSLA3) only released significantly more Man-containing carbohydrates compared to the Venus control. While the total Glc content remained similar, the amount of Man incorporated in AKI polymers increased up to 1 mg per well (2232 swap), which was 2.4-fold higher than AtCSLA2 and 1.6-fold higher than AkCSLA3 (Table S3). To reduce the background content of yeast β-1,3-glucans, AKI polymers from three biological replicates were pooled and treated with Zymolyase to isolate enriched heteromannan (EM), yielding 0.7–2.5 mg of HM for each CSLA construct (Table S3). Glycosidic linkage analysis confirmed that only AkCSLA3 and 3332 EM polymers contained significantly more 4-Glc compared to Venus and AtCSLA2 controls (Figure 4b and Table S3). To provide further evidence, we used HPAEC-PAD to profile the (gluco)mannan oligosaccharides released by partial endo-β-mannanase (E-BMABC) digestion from EM (Figure 4c and d) and commercial HM polysaccharides (Figure S4). While ivory nut mannan (INM) was digested to small manno-oligosaccharides (degree of polymerization, DP ≤ 4), konjac glucomannan (KGM) showed additional peaks with a retention time above the mannohexaose (DP 6) standard. These larger peaks, known to be diagnostic of glucomannan (Verhertbruggen *et al.*, 2021), represented only 1% of INM oligosaccharide area but 48% of KGM area (Figure 4c). Even when increasing the starting amount of INM, the digestion profiles did not resemble the glucomannan peaks of KGM (Figure S4). The *Pichia* AtCSLA2 and AkCSLA3 oligosaccharides resembled the digested INM and KGM standards, respectively (Figure 4d). While EM polymers from the chimeric 2322 and 2232 proteins showed detectable glucomannan peaks (4–7% of total oligosaccharide area; Figure 4d), they remained proportionally similar to AtCSLA2. Only the AkCSLA3 and 3332 *Pichia* material produced significant amounts of glucomannan oligosaccharides (22 to 26% of total area), albeit at half the level of the commercially available KGM standard (Figure 4c). Therefore, the second or third region of AkCSLA3, which contain its GT domain, are not sufficient to significantly alter the composition of mannan made by AtCSLA2.

Impact of CSLA Expression on Cell Growth

Next, we investigated how the linear (gluco)mannans produced by plant CSLA expression in *Pichia* cells impact yeast growth and morphology. None of the native or chimeric CSLA strains showed reduced growth compared to controls when cultivated in a non-inducible medium (Figure S5a). However, inoculation and cultivation of yeast in YPM (Figure S5b) or YPM+G (Figure S3b) medium led to a significant reduction of AkCSLA3 cell density compared to the Venus control. This growth inhibition was consistent in additional colonies, including those previously generated using the pPICZ B vector (Voiniciuc *et al.*, 2019), suggesting that the production of linear glucomannan by AkCSLA3 is toxic to the yeast cells. Multiple efforts to isolate stable *Pichia* transformants expressing AkCSLA3 under the control of *pGAP*, a strong constitutive promoter (Prielhofer *et al.*, 2017), were also unsuccessful. Strains expressing the 2322, 2232 or 3332 chimeric proteins showed similar growth curves as Venus and AtCSLA2 in YPM (Figure 5a). While cells expressing AkCSLA3 resembled the exponential growth of the other CSLA strains in the first 24 hours of cultivation, their optical density (OD) started to saturate earlier and remained at 30% lower values than the Venus control even after 60 h. Compared to OD600 curves, the fluorescence of the Venus protein control increased slower and reached a stable plateau 2–3 days of cultivation (Figure 5a).

After 24 h of induction, Venus and all CSLA cells showed similar morphology (Figure S5c) and area (Figure S5d) when stained with Trypan Blue (TB), which labels cell wall β-glucans (Liesche *et al.*, 2015). Since the growth curves showed the biggest difference after more than 2 days of cultivation (Figure 5a), we then examined how TB stains yeast cells after 72 h of growth in YPM+G. Surprisingly, at this timepoint, the majority of AkCSLA3 cells not only showed TB-stained walls but also appeared to be internally saturated with the fluorescent dye (Figure 5b). In contrast, only 4–6% of Venus and AtCSLA2 cells showed TB uptake (Figure S5e). Furthermore, prolonged expression of AkCSLA3 decreased the median cell area by 12.9% ($P < 0.00001$, one-way ANOVA with Tukey's pairwise), while AtCSLA2 increased it by 4.5% relative to the Venus control (Figure 5c). The 2322 and 2232 chimeric proteins led to intermediate cell dimensions compared to AkCSLA3 and the Venus control. TB is typically excluded by the plasma membrane (Figure S5c), and its uptake in a few Venus cells correlated with a loss of yellow fluorescence (Figure S5e). Partial spheroplasting of yeast cells using Zymolyase and β-mercaptoethanol led to impaired Venus cell shape and a loss of cytosolic yellow fluorescence (Figure 5d). While Zymolyase digestion had little effect on AkCSLA3 cells, this treatment elevated TB uptake in Venus and AtCSLA2 cells (Figure 5d). Therefore, extended AkCSLA3 expression reduced the growth and integrity of the yeast capsules, which could be at least partially restored by the chimeric 3332 glucomannan synthase.

To exclude that these histological defects are TB-specific and get further insight into the viability and cell wall morphology of engineered yeast after 3 days of cultivation, cells were stained with additional dyes. Calcofluor white (CF) was used to label yeast/plant β-glucans, and propidium iodide (PI) was used as a nuclear counterstain for dead cells. While CF is carbohydrate-specific, PI can penetrate cells with impaired membranes to intercalate nucleic acids (Suzuki *et al.*, 1997). Confocal laser scanning microscopy revealed differences in viability of the different CSLA strains (Figure 6). Compared to Venus, AtCSLA2, and 2232 cells, which rarely displayed nuclear staining, the ratio of PI- to CF-stained cells was increased by 27-fold following prolonged AkCSLA3 expression

(Figure 6c). Both 2322 and 3332 chimeric proteins, containing most of the AkCSLA3 GT domain, showed intermediate levels of PI uptake, but only 3332 expression reduced the area of CF-stained cells akin to AkCSLA3 (Figure 6b). These results were further supported by staining with congo red (CR), a β-glucan dye that has a higher affinity for HM polymers than CF (Wood, 1980). Like TB (Figure 5), CR staining was elevated in AkCSLA3 cells (Figure S6) and revealed a reduced cell area. In summary, AtCSLA2 increased the size of yeast cells with all wall stains tested (Figures 5, 6, and S6), while AkCSLA3 protein and/or glucomannan accumulation reduced cell growth and viability over time. In contrast to the *Pichia* platform, the transient expression of recombinant AkCSLA3-sYFP protein in *Nicotiana benthamiana* showed no signs of necrosis by 6 days post-infiltration (Figure S7). Therefore, yeast capsule properties can be tailored by modulating CSLA enzymes and hemicellulose production.

Approaches to Further Boost the HM Yield and Glc Content

In addition to being a suitable host for HM production, *Pichia* was previously used to make long or short β-1,4-glucans by expressing Arabidopsis CSLC4 with or without XXT1 (a xyloglucan xylosyltransferase), respectively (Cocuron *et al.*, 2007). We therefore used our optimized cultivation method to express two of the highest expressed GTs during nasturtium (*Tropaeolum majus*) seed development (Jensen *et al.*, 2012). TmCSLC4 alone produced 13% more Glc-containing AKI polymers than the Venus control, and even more (23%) glucan when co-expressed with TmXXT2 (Figure S8). It is noteworthy that the CSLC strains did not show the reduced growth observed for AkCSLA3 (Figure S8c), suggesting that its effects are glucomannan-specific. TmCSLC4, AtCSLA2 and AkCSLA3 share similar motifs in their GT2 domains (Figure 7a), including multiple amino acids involved in glucan coordination by a plant cellulose synthase complex (Purushotham *et al.*, 2020). We therefore tested if the second region of AtCSLA2 could be functionally exchanged with the corresponding GT2 sequence of TmCSLC4 (Figure S8a). Despite the 58% amino acid identity of the two regions, the 2422 construct was unable to make mannan nor increase Glc content (Figure S5b). We also did not detect any HM production by 2332 construct (Figure S9), which combines the two AkCSLA3 regions found in the high-yielding 2322 and 2232 chimeras (Figure 4). The introduction of a CSLC part and the exchange of a larger CSLA region were thus detrimental to hemicellulose biosynthesis. In contrast, the isolation of new 2232 transformants in the same experimental batch confirmed that this construct produced at least as much mannan as the native AtCSLA2 protein (Figure S9b).

Alignments of 14 active (gluco)mannan synthases (from angiosperms, gymnosperms, and a bryophyte; Figure S10) or of CSLAs with selected CSLC, CSLD, CSLF and cellulose synthase (CesA) proteins (Figure S11) did not pinpoint any polymorphisms associated with Glc incorporation in HM. Therefore, as an alternative strategy to boost (gluco)mannan production, we applied the MANNAN-SYNTHESIS RELATED (MSR) protein as a co-factor (Voiniciuc *et al.*, 2019). The top colonies for the AtCSLA2 and the 2322 and 2232 chimeric constructs were re-transformed with a linearized plasmid containing AtMSR1 under the control of the M-inducible *pDAS2* promoter. Assembled using GoldenPiCs, this new transcriptional unit contained an independent set of modular parts (regulatory

elements, selection marker, and genome integration site) to avoid homology with the previously integrated CSLAs. By introducing AtMSR1, the content of Man-containing AKI polymers became 1.5–3.0 times higher than the original, single-gene colonies (Figure 7b). These results were consistent with multiple independent transformants for each two-gene combinations. In this sequential transformation strategy, β-mannanase digestion of the AKI polymers released 1.9-fold more Man and 1.2-fold more Glc for the AtCSLA2 + AtMSR1 strain compared to AtCSLA2 alone (Figure 7c; $P < 0.05$), consistent with results obtained using a two-gene plasmid with recurring regulatory elements (Voiniciuc *et al.*, 2019). Interestingly, the co-expression of AtMSR1 with either 2322 or 2232 significantly increased HM production made, compared to original strains as well as the AtCSLA2 + AtMSR1 combination (Figure 7b and 7c). The enhanced HM content was most prominent for the 2322, which had a 1.5-fold increase in Glc and 3.1-fold increase in Man compared to AtCSLA2. This indicates that the AkCSLA3 GT domain portion can be directly or indirectly enhanced by AtMSR1 to a greater extent than the native AtCSLA2 sequence.

DISCUSSION

Plant cells are predominantly shaped and strengthened by a cellulose-hemicellulose network, which is built of a heterogeneous set of cross-linked that feature β-1,4-glycosidic bonds. In addition to these natural polysaccharides, which have been used by humans for centuries, microbes can now be modified to produce engineered living materials with entirely new functions (Gilbert and Ellis, 2019). In a recent landmark study, cellulose functionalized with enzymes or optogenetic sensors was produced by the co-culture of *Komagataeibacter rhaeticus* bacteria and engineered yeast (Gilbert *et al.*, 2021). In contrast to bacteria and yeast, plants have long generation times and increased biological complexity that dramatically limit the speed of design-build-test-learn cycles. In this study, we embarked on a quest to efficiently produce tailor-made HM polysaccharides in yeast, by exploring how swapping the domains from two CSLA enzymes from konjac (a monocot) and Arabidopsis (a dicot) modulate its yield and composition. In the developing konjac corm (Gille *et al.*, 2011), AkCSLA3 produces glucomannan that already has promising health care applications such as in the treatment of life style diseases (Behera and Ray, 2016). While AtCSLA2 is most important for seed mucilage biosynthesis in Arabidopsis (Yu *et al.*, 2014; Voiniciuc *et al.*, 2015), novel links between seed HM structure and salt tolerance provide an indication that fine-tuning HM structure could also be relevant for engineering stress-resistant crops (Yang *et al.*, 2020).

We also improved the speed of recombinant hemicellulose production in yeast relative to the sequential use of BMGY and BMMY cultivation media (Voiniciuc *et al.*, 2019), which are the standard conditions in *Pichia* studies. Our growth protocol yielded rapid HM synthesis along with a higher level of yeast glucans (Figure 2 and Figure 7b). Despite the elevated content of background Glc in AKI, glucomannan could be readily detected via β-mannanase release (Figure 4 and Figure 7c), linkage analysis (Figure 3), or following partial enzymatic removal of background yeast glucans. Glycosidic linkage analysis of AtCSLA2/AkCSLA3 chimeras showed that all the single-domain swaps produced at least some 4-linked Man, but five of the constructs had only a marginal increase compared to the trace amounts found in native *Pichia* polymers (Figure 2 and Figure S3). Except for the 3332

combination, N- or C-terminal domain swaps were not tolerated by CSLA enzymes as they led to significant less HM compared to the parents. Although AtCSLA2 and AkCSLA3 are predicted to have similar topologies, their termini are the regions with the most divergent sequences (Figure 1b) and may play outsized roles in the overall architecture of active (gluco)mannan synthases. Cellulose (Purushotham *et al.*, 2020), xyloglucan (Davis *et al.*, 2010), and β-1,3-1,4-linked-glucan (Jobling, 2015; Dimitroff *et al.*, 2016) synthases have been demonstrated or are predicted to form transmembrane pores that are important for glucan structure and translocation. Yet, the roles of the multiple transmembrane domains found in CSLAs remain to be elucidated, if their catalytic sites were to face the Golgi lumen.

We were surprised to find that 2322 and 2232 chimeric proteins produced higher amounts of mannan compared to AtCSLA2, without incorporating significant amounts of Glc like AkCSLA3 (Figure 4). Therefore, AtCSLA2 may have a strict requirement for AtMSR1 co-expression to produce glucomannan (Voiniciuc *et al.*, 2019). Larger AtCSLA2 domain swaps or the introduction of TmCSLC4 catalytic domain to boost Glc incorporation were not functional. One reason could be that CSLA glucomannan synthases have a strict requirement for GDP-Man and GDP-Glc donor sugars (Liepman *et al.*, 2005; Gille *et al.*, 2011), while CesA, CSLC and CSLFs utilize UDP-Glc (Pauly *et al.*, 2013). Since multiple efforts to generate fluorescently tagged versions of AtCSLA2 led to a loss of activity, the relative amounts or stability of the chimeric proteins (e.g. 2332 and 2422) could not be monitored. However, the addition of AtMSR1 enhanced HM production by the chimeric 2322 and 2232 proteins (Figure 7b,c). Therefore, we hypothesize that the MSR1 putative protein O-fucosyltransferase may directly interact with the GT2 domain of CSLA enzymes and/or glycosylate it.

A key advantage of our hemicellulose production system is that CSL enzymes can be stably integrated in the *Pichia* genome and their expression can be tightly controlled by inducible promoters. In two previous study of CSL chimeras, cereal CSLF6 proteins with swapped domains were transiently expressed by infiltrating *N. benthamiana* leaves and produced variable amounts (0.5–5.0% w/w) of β-1,3-1,4-linked-glucan (Dimitroff *et al.*, 2016; Jobling, 2015). Despite the variable yields, lichenase digestion of the mixed-linkage glucans released reproducible DP3:DP4 oligosaccharides ratios, which were typically similar to one of the parental enzymes or at an intermediate level (Dimitroff *et al.*, 2016; Jobling, 2015). If we similarly compared the relative Glc:Man ratios in several types of analyses (Figure 4), the top performing constructs could be divided into mannan (AtCSLA2, 2322 and 2232) and glucomannan (AkCSLA3 and 3332) synthases. While all the published CSLF6 chimeras were functional, five of our CSLA swaps showed significantly reduced activity compared (Figure 2). One possible explanation is that the cereal CSLF6s are closely related orthologs, but there is a greater distance between the CSLAs we selected. AkCSLA3 is orthologous to AtCSLA3 (Gille *et al.*, 2011), not AtCSLA2. Nevertheless, we could not pinpoint amino acids that are associated with glucomannan synthase activity (Figure S10). Given the strong effects of MSR1 protein co-expression (Figure 7), the Glc:Man ratio is clearly influenced by multiple factors. In the future, promising amino acid changes to enhance Glc incorporation could be predicted via *de novo* CSLA modelling, based on the structure of plant CesA (Purushotham *et al.*, 2020), and *in silico* sugar binding simulations.

Finally, we also evaluated the impact of CSLA expression on yeast cell growth and morphology and found that AkCSLA3 expression is toxic. While constitutive yeast promoters are available (Prielhofer *et al.*, 2017), we were not able to isolate stable colonies that constitutively express AkCSLA3. In contrast, AtCSLA2 and the chimeric enzymes producing relatively pure mannan showed no reductions in growth rates (Figure 5a). Despite the reduced biomass, AkCSLA3 cells were histologically indistinguishable from the controls after 24 h of induction. An overwhelming loss of viability (demonstrated by the uptake of TB, PI and CR stains) became evident for AkCSLA3 cells after three days of cultivation. However, the chimeric 3332 enzyme partially rescued these defects (Figure 5 and Figure 6), with only a small reduction in the Glc:Man ratio of its HM product (Figure 4). Furthermore, biomass accumulation was not reduced for the glucan synthase strains expressing CSLC4 (Figure S8), indicating that competition for UDP-Glc does not appear to be a problem. In contrast to its yeast effects, the transient expression of AkCSLA3 proteins in *N. benthamiana* leaves, where Man availability is limited, did not lead to any signs of cell death even at 6-days post-infiltration (Figure S7). We therefore hypothesize that the competition for GDP-Glc and/or high accumulation of glucomannan may explain this defect. The screening of natural or engineered CSLA variants that produce with higher levels of glucomannan than AkCSLA3 could be used to test this hypothesis. Additional tools will have to be developed to rapidly detect HM-producing colonies, because the dyes used to monitor yeast walls can bind cellulose, hemicelluloses, yeast β-glucans and chitin.

In conclusion, most of our HM-producing yeast strains grew well and showed a CSLA-dependent increase or decrease in cell size distribution. Therefore, they could be viewed as modular biological capsules for further engineering of polysaccharide-related pathways and/or for future biotechnological applications. Sensitive macromolecules such as therapeutic proteins can be protected by encapsulation in non-toxic plant polysaccharides (Vela Ramirez *et al.*, 2017). While plant biotechnology can offer low-cost solutions for drug production (Kwon and Daniell, 2015), *Pichia* cells are also attractive hosts for recombinant protein production and can be engineered to have a humanized glycosylation pathway (Jacobs *et al.*, 2009). Proteins produced in *Pichia* cells with wild-type walls have been mixed with food and were effective at reducing gastrointestinal bacterial infections in pigs (Virdi *et al.*, 2019), and face a simpler path to regulatory approval than genetically engineered plants. Therefore, we anticipate that yeast modification with plant GTs will provide a modular chassis for engineered biomaterials production and to encapsulate valuable cargo.

EXPERIMENTAL PROCEDURES

DNA Assembly, Verification and Transformation

Plant genes and swaps were cloned using the modular GoldenPiCs cloning system (Prielhofer *et al.*, 2017). The GoldenPiCS Kit was a gift from the Gasser/Mattanovich/Sauer group (Addgene kit #1000000133). All coding sequences were amplified with high-fidelity Phusion DNA Polymerase (Thermo Fisher Scientific) using the primers listed in Table S1. First, fragments were domesticated for Golden Gate assembly by introducing non-synonymous one or two base pair changes in custom fusion sites. One unwanted site in AtCSLA2 was domesticated by amplifying two fragments with 1F + dom1R and dom2F + 4R (Table S1). Three unwanted AkCSLA3 sites were domesticated by amplifying and fusing four fragments: 1F + dom1R, dom2F + dom2R, dom3F +

dom3R, and dom4F + 4R (Table S1). All Golden Gate assemblies were performed based to the GoldenPiCs methods (Prielhofer *et al.*, 2017), but using FastDigest restriction enzymes and T4 DNA ligase from Thermo Fisher Scientific. For each assembly, 10 µL reactions containing 25 ng of each DNA part were incubated for at least 5 cycles of digestion (5 min at 37°C) and ligation (10 min at 22°C), followed by final digestion and enzyme inactivation (10 min at 75°C) steps. DNA was transformed in *E. coli TOP10F'* via the heat-shock method. Antibiotic-resistant colonies were first verified by colony PCR using gene- and/or vector-specific genotyping primers in Table S1. DNA was isolated using the GeneJET Plasmid Miniprep Kit (ThermoFisher Scientific), and all BB1 coding sequences were verified by Sanger Sequencing with M13 primers and/or gene-specific primers. *pAOX1*:*CSL: RPP1Btt* transcriptional units were assembled in the BB3aZ_14 backbone. The *pDAS2*:*AtMSR1*:*RPBS2tt* transcriptional unit was first assembled in the BB2_BC vector, and was then fused with an empty *AB* cassette in *BB3rN_AC*, which has Nourseothricin resistance and integrates in the *RGI2* locus. BB3 plasmids were linearized, verified on a gel, and 150 ng of DNA was transformed into *Pichia pastoris X-33* via the condensed electroporation method (Lin-Cereghino *et al.*, 2005). After three days of cultivation, antibiotic-resistant colonies were re-streaked and verified by colony PCR using specific primers and Red Taq DNA polymerase master mix (VWR International).

Pichia Growth

Unless otherwise indicated, cells from at least three independent *Pichia* transformants per construct were grown for 48h in 2 mL Yeast-Peptone (YP) medium supplemented with M (1.5% v/v) dextrose (D, 2% w/v) and/or G (0.5% w/v) for biomass accumulation and induction. Polypropylene square 24-deepwell microplates (Enzyscreen CR1424a) with matching metal covers (CR1224b) served as re-usable cultivation vessels, which were washed and sterilized by autoclaving. Plates, sealed with micropore tape, were incubated at 30°C and 250 rpm in a shaking incubator (Thermo Scientific MaxQ 6000). After incubation, cultures were transferred to 2 mL tubes and the cells were collected by centrifugation for 5 min at 2000 *g*.

To measure growth curves, two biological replicates of each genotype were pre-cultured in 2 mL YPD medium in 14 mL sterile glass culture tubes with aluminum caps. Cultures were incubated for 24 hours at 30°C and 250 rpm in a shaking incubator (Thermo Scientific MaxQ 6000). After incubation, each pre-culture was diluted 1:10 and the OD600 was measured with the BioSpectrometer (Eppendorf). The OD was then adjusted to 0.1 in YPM medium and three replicates with 300 µL of each pre-culture were transferred to a 48-sterile well plate and mixed (360 rpm, 1.5 mm orbital amplitude) inside a fluorescent plate reader (Tecan Spark 10M) at 29 °C. After every 30 min of mixing, absorbance at 600 nm and fluorescence (excitation 485 ± 10 nm, emission at 530 ± 12.5 nm, manual gain = 50) were recorded multiple times per well (5 x 5, filled circle pattern, 700 µm border).

Isolation and Analyses of Carbohydrate Polymers

AKI polymers were obtained as previously described (Voiniciuc *et al.*, 2019), but using cell pellets as starting material and a thermomixer from a different supplier (neoMix 7-921). After neutralization and washing, AKI polymers were homogenized in 600 µL of water using a ball mill, and

aliquots of the material were analyzed immediately or were stored as described below. For EM isolation, AKI samples were pooled from three biological replicates, pelleted by centrifugation, and re-suspended in 300 µL of 0.2 M potassium phosphate buffer (pH 7.0). After re-suspension, β-1,3-glucans were digested by adding 300 µL of water containing 125 µg of Zymolyase 20 T (from *Arthrobactor lutes*; USBiological) and 10 µg sodium azide. The samples were mixed for 48 h at 37 °C and 250 rpm in an incubator (Thermo Scientific MaxQ 6000). After centrifugation for 5 min at 16,000 *g*, the remaining EM insoluble pellet was washed twice with 1 mL of water before carefully mixing it with 300 µL of acetone and gently dried to avoid material loss. EM polymers were homogenized in 1000 µL of water using a ball mill. All carbohydrate samples and standards were analyzed immediately or were stored at 4°C (several days) or at -20°C (long-term).

Quantification of Monosaccharides and Oligosaccharides

For total monosaccharide quantification, 50 µL of *Pichia* AKI material or standards were mixed with 800 µL of 30 µg/mL Ribose solution (internal standard). Blank and sugar standards containing galactose, Man and Glc were prepared similarly. All samples and standards were hydrolyzed by adding 30 µL of 72% (w/w) sulfuric acid, mixing and then incubating for 60 min at 120°C in heat blocks. After cooling to room temperature, all tubes were centrifuged for 15 min at 20,000 *g* to pellet any particles that remained insoluble, and 10 µL of the supernatant was injected for HPAEC-PAD analysis. Carbohydrates were separated using a Metrohm 940 Professional IC Vario system equipped with Metrosep Carb 2-250/4.0 analytical and guard columns. A short 30 min protocol suitable for separation of the three HM sugar components (galactose, Glc and Man) included a 20 min isocratic 2 mM sodium hydroxide (NaOH) + 3.4 mM sodium acetate (NaAce) separation step, followed by 3 min rinse with 80 mM NaOH + 136 mM NaAce, before 4 min re-equilibration with the starting eluents. Trace amounts of glucosamine were detected but were not quantified. Peaks were automatically integrated and calibrated, with manual correction when necessary, using the MagIC Net 3.2 software (Metrohm).

For the digestion followed by monosaccharide analysis, 50 µL of *Pichia* AKI suspension were incubated for 30 min at 40 °C and 1000 rpm in a thermomixer (neoMix 7-921) in 100 µL of 0.2 M potassium phosphate buffer (pH 7.0) containing 1 U of endo-1,4-β-Mannanase (Megazyme, E-BMABC). After incubation, samples were centrifuged for 2 min at 20,000 *g* and 100 µL of the supernatant was dried under pressurized air using a heat block concentrator (Techne Dri Block DB200/3). Dry samples and standards were hydrolyzed with 150 µL of 2 M trifluoroacetic acid (TFA) for 90 min at 120°C. After cooling to room temperature, hydrolyzed samples were briefly centrifuged and dried once again. Residual TFA was removed by washing with 300 µL of isopropanol and dried as above. Samples were then eluted in 400 µL of 30 µg/mL Ribose solution (internal standard) and were centrifuged for 2 min at 20,000 *g* prior to transferring 100 µL of supernatant to IC vials.

For oligosaccharide profiling, 100 µL of potassium phosphate buffer (pH 7.0) containing 0.1 U of E-BMABC enzyme were added to 100 µL of enriched AKI or polysaccharide standards (from Megazyme) and incubated for 30 min at 40 °C and 1500 rpm in a thermomixer. Enzyme was then heat-inactivated for 10 min at 90 °C and 1500 rpm. Samples were centrifuged for 2 min at 20,000 *g*

and 10 µL of the supernatant were injected for HPAEC-PAD profiling of oligosaccharides. The instrument and column setup were the same as for monosaccharide analysis but utilized a different eluent gradient. Starting with 15.6 mM NaOH, the gradient was increased to 78 mM NaOH over 5 min, followed by a linear increase to 78 mM NaOH + 50 mM NaAce for 25 min. The column was re-equilibrated for 15 min with 15.6 mM NaOH, before the next sample was injected.

Linkage analysis

For glycosidic linkage analysis of polysaccharides, 100 µL of AKI or EM polysaccharides were methylated, hydrolyzed, reduced and acetylated to generate partially methylated alditol acetates (Ciucanu and Kerek, 1984). After derivatization, 2 µL of each sample was automatically injected for gas chromatography–mass spectrometry. We used an Agilent Technologies 6890N GC system equipped with a Supelco SP-2380 column (30 m x 0,25 mm x 0,2 µm) and coupled to an Agilent 5975 quadrupole EI detector. The peak areas of partially methylated alditol acetates were semi-automatically integrated in Agilent MSD Chemstation Classic Data Analysis (G1701FA) based on their retention time and relative ion spectra of polysaccharide standards.

Fluorescence microscopy

For microscopy, cell cultures diluted in water or phosphate-buffered saline (PBS) solution, pH 7.0, and mixed with an equal volume of 0.01% (w/v) solution of one or more dyes (all from Sigma Aldrich, except Calcofluor White from Megazyme). Cells were imaged with a 40x or 60x objectives on a laser scanning confocal microscope (Carl Zeiss, LSM 700), beam splitter (MBS 405/488/555/639), and multiple laser/filter combinations. Separate acquisition tracks with the following excitation and emission wavelengths were used to acquire Venus fluorescence (488 nm and BP 450-550), CF (405 nm and BP 420-550), TB and PI (639 nm and LP 640 for both). Images were acquired using the ZEN 2011 (black edition) from Carl Zeiss and then processed uniformly in ImageJ (Schindelin *et al.*, 2012). To quantify cell numbers and sizes, the microscopy images were segmented using the web version (http://yeastspotter.csb.utoronto.ca) of the YeastSpotter tool (Lu *et al.*, 2019), and particles were then measured in ImageJ with the Analyze Particles (size=3-40, circularity=0.80-1.00) command.

Transient expression in *N. benthamiana* leaves

For plant expression, the coding sequences were synthesized and were cloned in the previously described *pCV01* vector (Voiniciuc *et al.*, 2015), using the LIC primers listed in Table S1 and ligation independent cloning (De Rybel *et al.*, 2011). Constructs were verified via Sanger sequencing. Transient expression was performed in *N. benthamiana* leaves as previously described (Grefen *et al.*, 2010). *Agrobacterium tumefaciens* strains containing the desired gene of interest were mixed with the P19 viral suppressor (each with an OD600 of 0.7). *Agrobacterium* mixtures were infiltrated in the lower side of the leaf of 5-week-old plants. A total of eight replicate infiltration spots for each gene were distributed randomly in leaves from four different plants to avoid positional bias. The subcellular yellow fluorescence was analyzed after 4 days using similar confocal microscope setup to the described yeast Venus imaging. Whole leaves were imaged at 6-days post-infiltration using a

hand-held camera as well as a gel documentation system (Analytik Jena, UVP Gelstudio Plus) equipped with an overhead blue LED and a GFP Emission Filter (#849-00405-0).

ACKNOWLEDGEMENTS

The Designer Glycans group was funded by the Leibniz Institute of Plant Biochemistry and the Deutsche Forschungsgemeinschaft (DFG, German Research Foundation grant 414353267 to CV). Additional funding was provided by the DFG under Germany's Excellence Strategy—EXC 2048/1—Project ID: 390686111 to MP. Mehdi Ben Targem assisted with CSLA sequence domestication and Annika Grieß-Osowski prepared the *Agrobacterium AkCSLA3* strain. Balakumaran Chandrasekar and Niklas Gawenda (Institute for Plant Cell Biology and Biotechnology) kindly provided the two glucan-producing *Pichia* control strains. We gratefully acknowledge the following individuals and groups at the Leibniz Institute of Plant Biochemistry for instrument access: GC-MS (Karin Gorzolka, Department of Biochemistry of Plant Interactions), confocal microscope (Bettina Hause, Imaging Unit of the IPB), and plate readers (Martin Weissenborn, Bioorganic Chemistry group and Steffen Abel, Department of Molecular Signal Processing). Pascal Püllmann provided useful tips on high-throughput yeast growth, and gardeners from the IPB Experimental Nursery group assisted with the tobacco cultivation.

AUTHOR CONTRIBUTIONS

MP proposed the domain swap strategy. CV designed and coordinated all experiments. JW and FS assembled the AtCSLA2/AkCSLA3 single domain swaps and carried out the initial activity screen. MR performed all the presented experiments with help from CV, except that the Figure S7 work was done by BY. CV and MR wrote the paper and prepared the figures/tables with input from all authors.

CONFLICT OF INTEREST

The authors declare no conflict of interest.

DATA AVAILABILITY STATEMENT

All relevant data can be found within the manuscript and its supporting materials.

FIGURE LEGENDS

Figure 1. Modular engineering of hemicellulose synthesis. (a) Model of the potential cell phenotypes and future applications, such as biological capsules for therapeutic proteins, of yeast engineered to produce plant matrix polysaccharides. (b) Topology of AtCSLA2 and AkCSLA3 enzymes visualized with TOPCONS 2.0. Transmembrane domains (pink boxes), and regions inside (red) and outside (blue) the membrane. The GT2 domain denotes the conserved GT2 domain (Pfam PF13641). Three regions (dashed lines) with 100% amino acid identity were selected as borders for CSLA domain swapping. (c) Workflow for the assembly of chimeric DNA using the GoldenPICS cloning system. CSL domains are fused seamlessly in a level 1 vector, and then assembled with a yeast promoter and a transcriptional terminator into a level 2 vector for stable yeast transformation. Selected yeast colonies were induced to express the CSL enzymes using methanol and were subjected to cell wall analyses. (d) Matrix and labeling of AtCSLA2/AkCSLA3 single domain swaps assembled in this study.

Figure 2. Abundance and composition of engineered wall polymers. Absolute monosaccharide composition of alkaline-insoluble polymers after cultivation of engineered yeast strains in two media: (a) YPM (containing 1.5% w/w Methanol as sole carbon source) or (b) YPM + G (plus 0.5% v/v Glycerol to boost biomass accumulation. Polysaccharides were hydrolyzed using sulfuric acid. For

each sugar, dots show the values of two biological replicates, and different letters denote significant changes (one-way ANOVA with Tukey test, $P < 0.05$). All samples in (b) had similar Glc levels.

Figure 3. Effects of AtCSLA2 and AkCSLA3 domain swaps on (gluco)mannan linkages. Relative amounts of 1,4-linked Man (a) and 1,4-linked Glc (b) residues, as a percentage of total glycosidic linkages detected after derivatization to partially methylated alditol acetates. The 4-Glc background level is derived from native yeast polymers such as glycogen. Jitter plots show three biological replicates. Boxes show the 25–75% quartiles, the median value (inner horizontal line), and whiskers extending to the largest/smallest values. Different letters denote significant changes (one-way ANOVA with Tukey test, $P < 0.05$).

Figure 4. Structure of (gluco)mannans produced by the top chimeric CSLAs. (a) Carbohydrates released by endo-β-1,4-mannanase digestion of alkaline-insoluble polymers. Solubilized carbohydrates were subjected to TFA-hydrolysis prior to HPEAC-PAD analysis. Data show the mean + SD of three biological replicates, re-grown based on the most promising *Pichia* strains from Figures 2 and 3. (b) Relative abundance of glucomannan glycosidic linkages in enriched mannan (EM) samples after Zymolyase treatment. Data show the mean + SD of three measurements for each sample. (c) Relative peak area of mannan (Man_{1-5}) and glucomannan (GlcMan) oligosaccharides released from *Pichia* EM by mannanase relative to ivory nut mannan (INM) and konjac glucomannan (KGM) standards. Data show the mean + SD of two measurements. Different letters in (a) to (c) denote significant changes (one-way ANOVA with Tukey test, $P < 0.05$). (d) HPAEC-PAD oligosaccharide profiles of mannanase-treated samples quantified in panel (c). GlcMan diagnostic peaks, based on the controls in Figure S4, are marked by asterisks.

Figure 5. CSLA expression influences yeast growth and cell wall morphology. (a) Growth curve of CSLA parents and top swaps after transfer to YPM in a 48-well plate. Optical density at 600 nm (OD600) and yellow relative fluorescence units (RFU) were monitored with a plate reader after every 30 min of shaking. Data show the mean ± SD of at least 3 biological replicates. The error bars are only shown for Venus and AkCSLA3 due to space constraints, but data points had a coefficient of variance below 5% after 32 h. (b) Morphology of yeast cells stained with Trypan Blue (TB) after 72 h of cultivation in YPM + G. (c) Yeast cell area (µm²) of CSLA parents and top swaps. Violin plot shows the size distribution of at least 350 cells per genotype. Different letters denote significant changes (one-way ANOVA with Tukey test, $P < 0.0001$). (d) Zymolyase and β-mercaptoethanol treatment spheroplasted Venus cells based on Transmitted Light (TL) and yellow protein fluorescence (YFP) imaging. Scale bars = 5 µm in (b) and 10 µm in (d). Arrows indicate TB uptake.

Figure 6. Glucomannan synthesis by AkCSLA3 is toxic to yeast cells. (a) Transmitted light (TL), calcofluor white (CF), and propidium iodide (PI) staining of cells after 72 h of cultivation in YPM + G. Scale bars = 5 µm. (b) Yeast cell area (µm²) of CSLA parents and top swaps. Violin plot shows the size distribution of at least 1200 cells per genotype (combining four biological replicates). Different letters denote significant changes (one-way ANOVA with Tukey test, $P < 0.001$). (c) The ratio of cells stained with PI relative to those stained with CF, segment using Yeastspotter and counted with ImageJ. Dots show four biological replicates. Boxes show the 25–75% quartiles, the median value (inner horizontal line), and whiskers extending to the largest/smallest values. Different letters denote significant changes (one-way ANOVA with Tukey test, $P < 0.05$).

Figure 7. CSL Enzyme Features and Further Enhancement of Hemicellulose Synthesis. (a) Multiple sequence alignment, showing the selected borders for the chimeric proteins (dashed lines) and additional conserved motifs among active CSLAs (green lines). Arrowheads mark residues involved in glucan coordination by the structural studies of the PttCesA8 enzyme in *Pichia*. The shading is proportional to the amino acid similarity. TM, transmembrane domains. (b) Swapped CSLA domains are particularly boosted by catalytic domain by AtMSR1 to surpass parental yields, based on absolute monosaccharide composition. (b) Monosaccharide composition of carbohydrates released from AKI by β-mannanase digestion. In (b) and (c), dots show two technical replicates, measured in duplicate. Different letters denote significant changes (one-way ANOVA with Tukey test, $P < 0.05$).

SUPPORTING INFORMATION

Figure S1. Sanger sequencing alignments of assembled *CSL* constructs.
Figure S2. Genotyping of domain-swapped AtCSLA2/AkCSLA3 yeast colonies.

REFERENCES

Behera, S.S. and Ray, R.C. (2016) Konjac glucomannan, a promising polysaccharide of Amorphophallus konjac K. Koch in health care. *Int. J. Biol. Macromol.*, **92**, 942–956.

Berglund, J., Kishani, S., Morais de Carvalho, D., Lawoko, M., Wohlert, J., Henriksson, G., Lindström, M.E., Wågberg, L. and Vilaplana, F. (2020) Acetylation and Sugar Composition Influence the (In)Solubility of Plant β-Mannans and Their Interaction with Cellulose Surfaces. *ACS Sustain. Chem. Eng.*, **8**, 10027–10040.

Bewley, J.D., Bradford, K.J., Hilhorst, H.W.M. and Nonogaki, H. (2013) Structure and Composition. In J. D. Bewley, K. J. Bradford, H. W. M. Hilhorst, and H. Nonogaki, eds. *Seeds*. New York, NY: Springer New York, pp. 1–25.

Buckeridge, M.S. (2010) Seed cell wall storage polysaccharides: models to understand cell wall biosynthesis and degradation. *Plant Physiol.*, **154**, 1017–1023.

Ciucanu, I. and Kerek, F. (1984) A simple and rapid method for the permethylation of carbohydrates. *Carbohydr. Res.*, **131**, 209–217.

Cocuron, J.-C., Lerouxel, O., Drakakaki, G., Alonso, A.P., Liepman, A.H., Keegstra, K., Raikhel, N. and Wilkerson, C.G. (2007) A gene from the cellulose synthase-like C family encodes a -1,4 glucan synthase. *Proc. Natl. Acad. Sci.*, **104**, 8550–8555.

Collins, H.M., Burton, R.A., Topping, D.L., Liao, M., Bacic, A. and Fincher, G.B. (2010) REVIEW: Variability in Fine Structures of Noncellulosic Cell Wall Polysaccharides from Cereal Grains: Potential Importance in Human Health and Nutrition. *Cereal Chem.*, **87**, 272–282.

Davis, J., Brandizzi, F., Liepman, A.H. and Keegstra, K. (2010) Arabidopsis mannan synthase CSLA9 and glucan synthase CSLC4 have opposite orientations in the Golgi membrane. *Plant J. Cell Mol. Biol.*, **64**, 1028–1037.

De Rybel, B., Berg, W. van den, Lokerse, A., Liao, C.-Y., Mourik, H. van, Möller, B., Peris, C.L. and Weijers, D. (2011) A Versatile Set of Ligation-Independent Cloning Vectors for Functional Studies in Plants. *Plant Physiol.*, **156**, 1292–1299.

Dimitroff, G., Little, A., Lahnstein, J., Schwerdt, J.G., Srivastava, V., Bulone, V., Burton, R.A. and Fincher, G.B. (2016) (1,3;1,4)-β-Glucan Biosynthesis by the CSLF6 Enzyme: Position and Flexibility of Catalytic Residues Influence Product Fine Structure. *Biochemistry*, **55**, 2054–2061.

Engler, C., Kandzia, R. and Marillonnet, S. (2008) A One Pot, One Step, Precision Cloning Method with High Throughput Capability. *PLOS ONE*, **3**, e3647.

Gilbert, C. and Ellis, T. (2019) Biological Engineered Living Materials: Growing Functional Materials with Genetically Programmable Properties. *ACS Synth. Biol.*, **8**, 1–15.

Gilbert, C., Tang, T.-C., Ott, W., Dorr, B.A., Shaw, W.M., Sun, G.L., Lu, T.K. and Ellis, T. (2021) Living materials with programmable functionalities grown from engineered microbial co-cultures. *Nat. Mater.*, https://doi.org/10.1038/s41563-020-00857-5.

Gille, S., Cheng, K., Skinner, M.E., Liepman, A.H., Wilkerson, C.G. and Pauly, M. (2011) Deep sequencing of voodoo lily (Amorphophallus konjac): An approach to identify relevant genes involved in the synthesis of the hemicellulose glucomannan. *Planta*, **234**, 515–526.

Grefen, C., Donald, N., Hashimoto, K., Kudla, J., Schumacher, K. and Blatt, M.R. (2010) A ubiquitin-10 promoter-based vector set for fluorescent protein tagging facilitates temporal stability and native protein distribution in transient and stable expression studies. *Plant J.*, **64**, 355–365.

Jacobs, P.P., Geysens, S., Vervecken, W., Contreras, R. and Callewaert, N. (2009) Engineering complex-type N-glycosylation in Pichia pastoris using GlycoSwitch technology. *Nat. Protoc.*, **4**, 58–70.

Jensen, J.K., Schultink, A., Keegstra, K., Wilkerson, C.G. and Pauly, M. (2012) RNA-Seq Analysis of Developing Nasturtium Seeds (Tropaeolum majus): Identification and Characterization of an Additional Galactosyltransferase Involved in Xyloglucan Biosynthesis. *Mol. Plant*, **5**, 984–992.

Jobling, S.A. (2015) Membrane pore architecture of the CslF6 protein controls (1-3,1-4)-β-glucan structure. *Sci. Adv.*, **1**, e1500069.

Kim, S.-J., Chandrasekar, B., Rea, A.C., et al. (2020) The synthesis of xyloglucan, an abundant plant cell wall polysaccharide, requires CSLC function. *Proc. Natl. Acad. Sci.*, **117**, 20316–20324.

Kwon, K.-C. and Daniell, H. (2015) Low-cost oral delivery of protein drugs bioencapsulated in plant cells. *Plant Biotechnol. J.*, **13**, 1017–1022.

Liepman, A.H., Wilkerson, C.G. and Keegstra, K. (2005) Expression of cellulose synthase-like (Csl) genes in insect cells reveals that CslA family members encode mannan synthases. *Proc. Natl. Acad. Sci. U. S. A.*, **102**, 2221–2226.

Liesche, J., Marek, M. and Günther-Pomorski, T. (2015) Cell wall staining with Trypan blue enables quantitative analysis of morphological changes in yeast cells. *Front. Microbiol.*, **6**, 107.

Lin-Cereghino, J., Wong, W.W., Xiong, S., Giang, W., Luong, L.T., Vu, J., Johnson, S.D. and Lin-Cereghino, G.P. (2005) Condensed protocol for competent cell preparation and transformation of the methylotrophic yeast Pichia pastoris. *BioTechniques*, **38**, 44, 46, 48.

Lu, A.X., Zarin, T., Hsu, I.S. and Moses, A.M. (2019) YeastSpotter: accurate and parameter-free web segmentation for microscopy images of yeast cells. *Bioinformatics*, **35**, 4525–4527.

Pauly, M., Gawenda, N., Wagner, C., Fischbach, P., Ramírez, V., Axmann, I.M. and Voiniciuc, C. (2019) The Suitability of Orthogonal Hosts to Study Plant Cell Wall Biosynthesis. *Plants*, **8**, 516.

Pauly, M., Gille, S., Liu, L., Mansoori, N., Souza, A. de, Schultink, A. and Xiong, G. (2013) Hemicellulose biosynthesis. *Planta*, **238**, 627–642.

Prielhofer, R., Barrero, J.J., Steuer, S., et al. (2017) GoldenPiCS: a Golden Gate-derived modular cloning system for applied synthetic biology in the yeast Pichia pastoris. *BMC Syst. Biol.*, **11**, 123.

Purushotham, P., Ho, R. and Zimmer, J. (2020) Architecture of a catalytically active homotrimeric plant cellulose synthase complex. *Science*, **369**, 1089–1094.

Scheller, H.V. and Ulvskov, P. (2010) Hemicelluloses. *Annu. Rev. Plant Biol.*, **61**, 263–289.

Schindelin, J., Arganda-Carreras, I., Frise, E., et al. (2012) Fiji: an open-source platform for biological-image analysis. *Nat. Methods*, **9**, 676–682.

Suzuki, T., Fujikura, K., Higashiyama, T. and Takata, K. (1997) DNA Staining for Fluorescence and Laser Confocal Microscopy. *J. Histochem. Cytochem.*, **45**, 49–53.

Tsirigos, K.D., Peters, C., Shu, N., Käll, L. and Elofsson, A. (2015) The TOPCONS web server for consensus prediction of membrane protein topology and signal peptides. *Nucleic Acids Res.*, **43**, W401-407.

Vela Ramirez, J.E., Sharpe, L.A. and Peppas, N.A. (2017) Current state and challenges in developing oral vaccines. *Adv. Drug Deliv. Rev.*, **114**, 116–131.

Verhertbruggen, Y., Bouder, A., Vigouroux, J., et al. (2021) The TaCslA12 gene expressed in the wheat grain endosperm synthesizes wheat-like mannan when expressed in yeast and Arabidopsis. *Plant Sci.*, **302**, 110693.

Virdi, V., Palaci, J., Laukens, B., Ryckaert, S., Cox, E., Vanderbeke, E., Depicker, A. and Callewaert, N. (2019) Yeast-secreted, dried and food-admixed monomeric IgA prevents gastrointestinal infection in a piglet model. *Nat. Biotechnol.*, **37**, 527–530.

Voiniciuc, C., Dama, M., Gawenda, N., Stritt, F. and Pauly, M. (2019) Mechanistic insights from plant heteromannan synthesis in yeast. *Proc. Natl. Acad. Sci.*, **116**, 522–527.

Voiniciuc, C., Schmidt, M.H.-W., Berger, A., Yang, B., Ebert, B., Scheller, H.V., North, H.M., Usadel, B. and Günl, M. (2015) MUCILAGE-RELATED10 Produces Galactoglucomannan That Maintains Pectin and Cellulose Architecture in Arabidopsis Seed Mucilage. *Plant Physiol.*, **169**, 403–420.

Wood, P.J. (1980) Specificity in the interaction of direct dyes with polysaccharides. *Carbohydr. Res.*, **85**, 271–287.

Yang, B., Hofmann, F., Usadel, B. and Voiniciuc, C. (2020) Seed hemicelluloses tailor mucilage properties and salt tolerance. *New Phytol.*, **229**, 1946–1954.

Yu, L., Lyczakowski, J.J., Pereira, C.S., Kotake, T., Yu, X., Li, A., Mogelsvang, S., Skaf, M.S. and Dupree, P. (2018) The Patterned Structure of Galactoglucomannan Suggests It May Bind to Cellulose in Seed Mucilage. *Plant Physiol.*, **178**, 1011–1026.

Yu, L., Shi, D., Li, J., et al. (2014) CELLULOSE SYNTHASE-LIKE A2, a glucomannan synthase, is involved in maintaining adherent mucilage structure in arabidopsis seed. *Plant Physiol.*, **164**, 1842–1856.

Zhong, R., Cui, D. and Ye, Z. (2019) Evolutionary origin of O-acetyltransferases responsible for glucomannan acetylation in land plants. *New Phytol.*, **224**, 466–479.

Zhong, R., Cui, D. and Ye, Z.-H. (2018) Members of the DUF231 Family are O-Acetyltransferases Catalyzing 2-O- and 3-O-Acetylation of Mannan. *Plant Cell Physiol.*, **59**, 2339–2349.

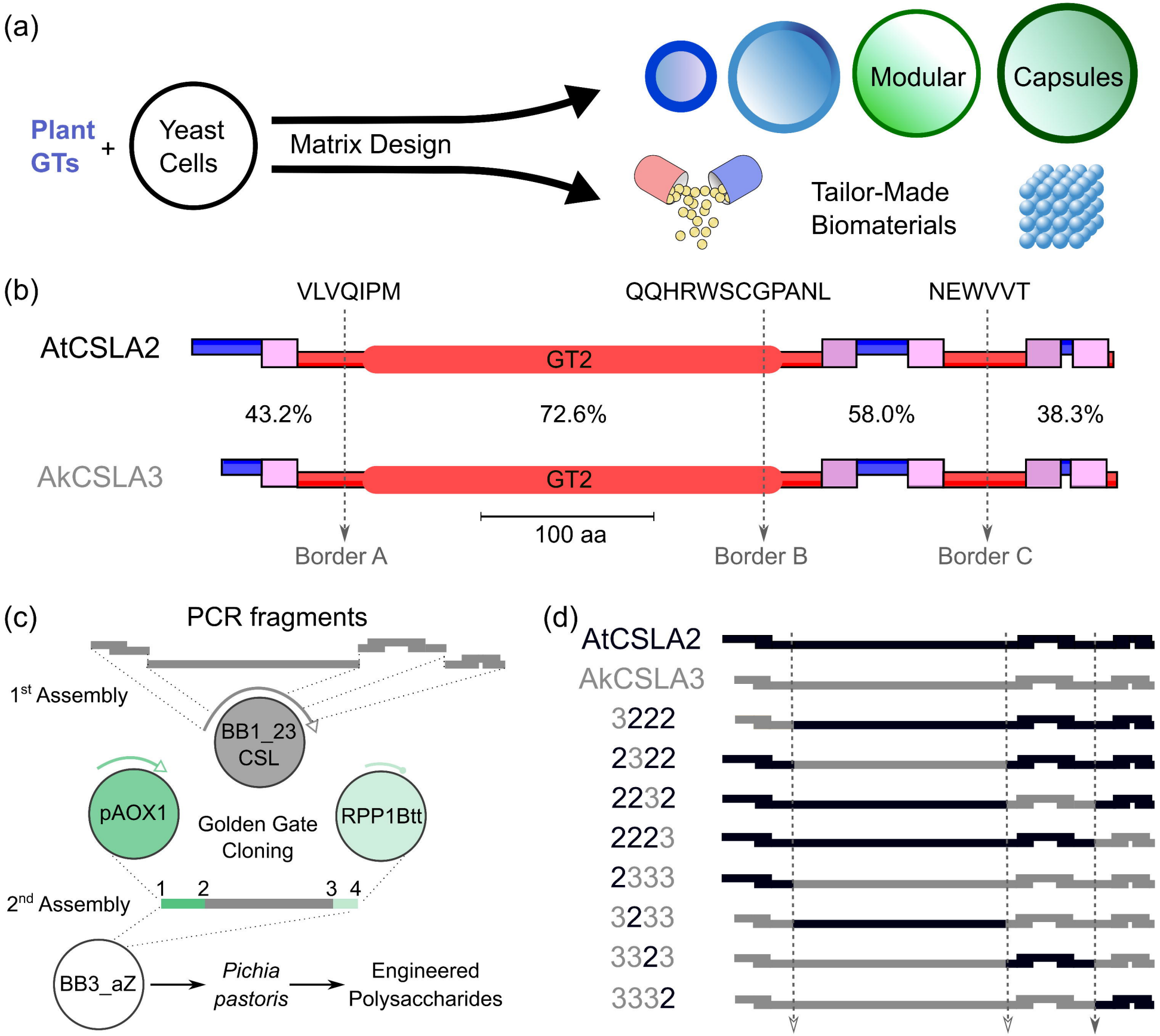
(a)
Plant GTs
+
Yeast Cells
Matrix Design
Modular
Capsules
Tailor-Made Biomaterials
(b)
VLVQIPM
QQHRWSCGPANL
NEWVVT
AtCSLA2
GT2
43.2%
72.6%
58.0%
38.3%
AkCSLA3
GT2
100 aa
Border A
Border B
Border C
(c)
PCR fragments
1st Assembly
BB1_23 CSL
pAOX1
Golden Gate Cloning
RPP1Btt
2nd Assembly
1
2
3
4
BB3_aZ
Pichia pastoris
Engineered Polysaccharides
(d)
AtCSLA2
AkCSLA3
3222
2322
2232
2223
2333
3233
3323
3332

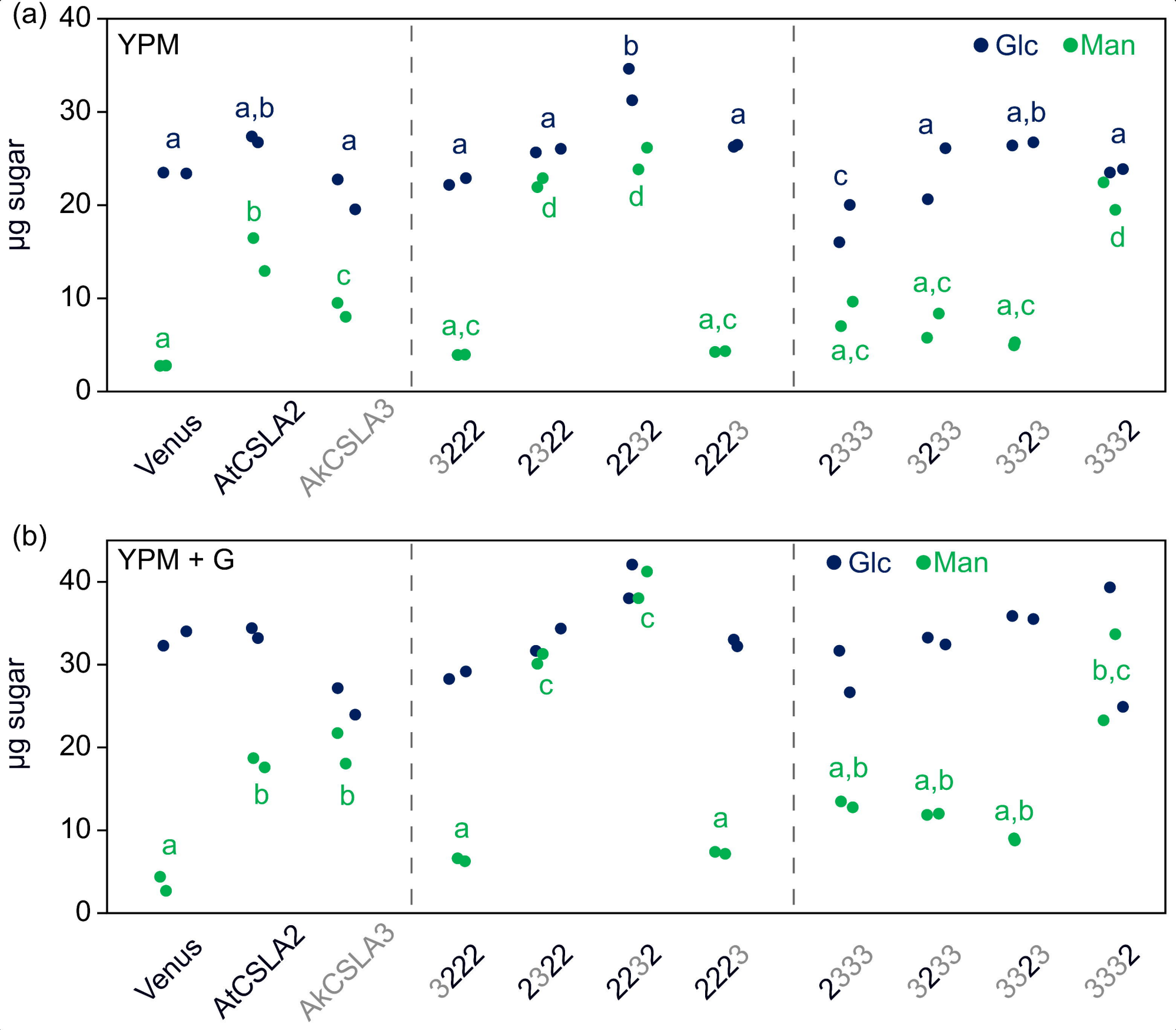
(a)
YPM
Glc
Man
µg sugar
0
10
20
30
40
a
a,b
a
b
c
a
a
a
b
d
a
a,c
a,c
c
a
a,b
a,c
a,c
a
Venus
AtCSLA2
AkCSLA3
3222
2322
2232
2223
2333
3233
3323
3332
(b)
YPM + G
Glc
Man
µg sugar
0
10
20
30
40
a
b
b
a
c
c
a
a
a,b
a,b
a,b
b,c
Venus
AtCSLA2
AkCSLA3
3222
2322
2232
2223
2333
3233
3323
3332

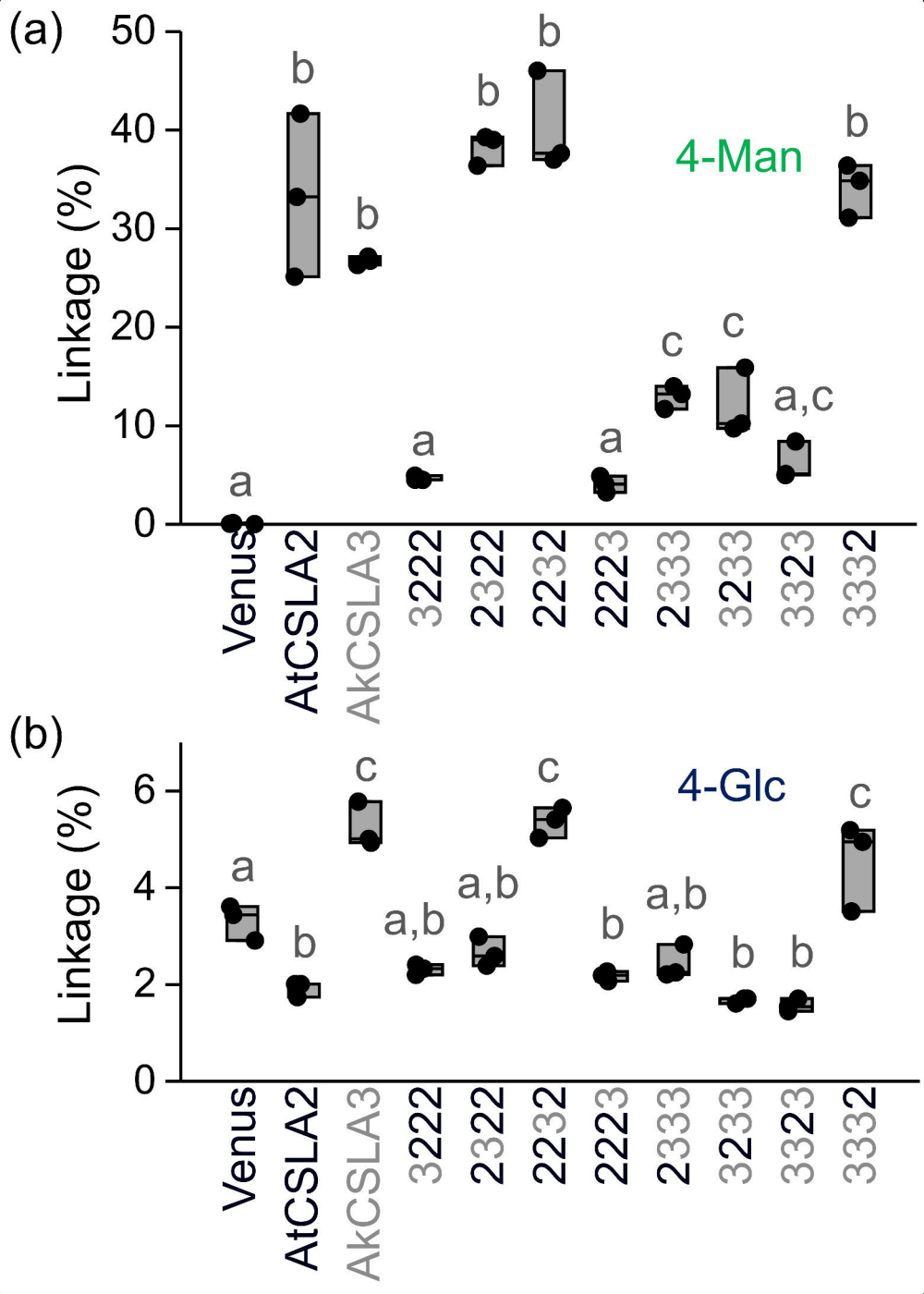
(a)
Linkage (%)
50
40
30
20
10
0
4-Man
a
b
b
a
b
b
a
c
c
a,c
b
Venus
AtCSLA2
AkCSLA3
3222
2322
2232
2223
2333
3233
3323
3332
(b)
Linkage (%)
6
4
2
0
4-Glc
a
b
c
a,b
a,b
c
b
a,b
b
b
c
Venus
AtCSLA2
AkCSLA3
3222
2322
2232
2223
2333
3233
3323
3332

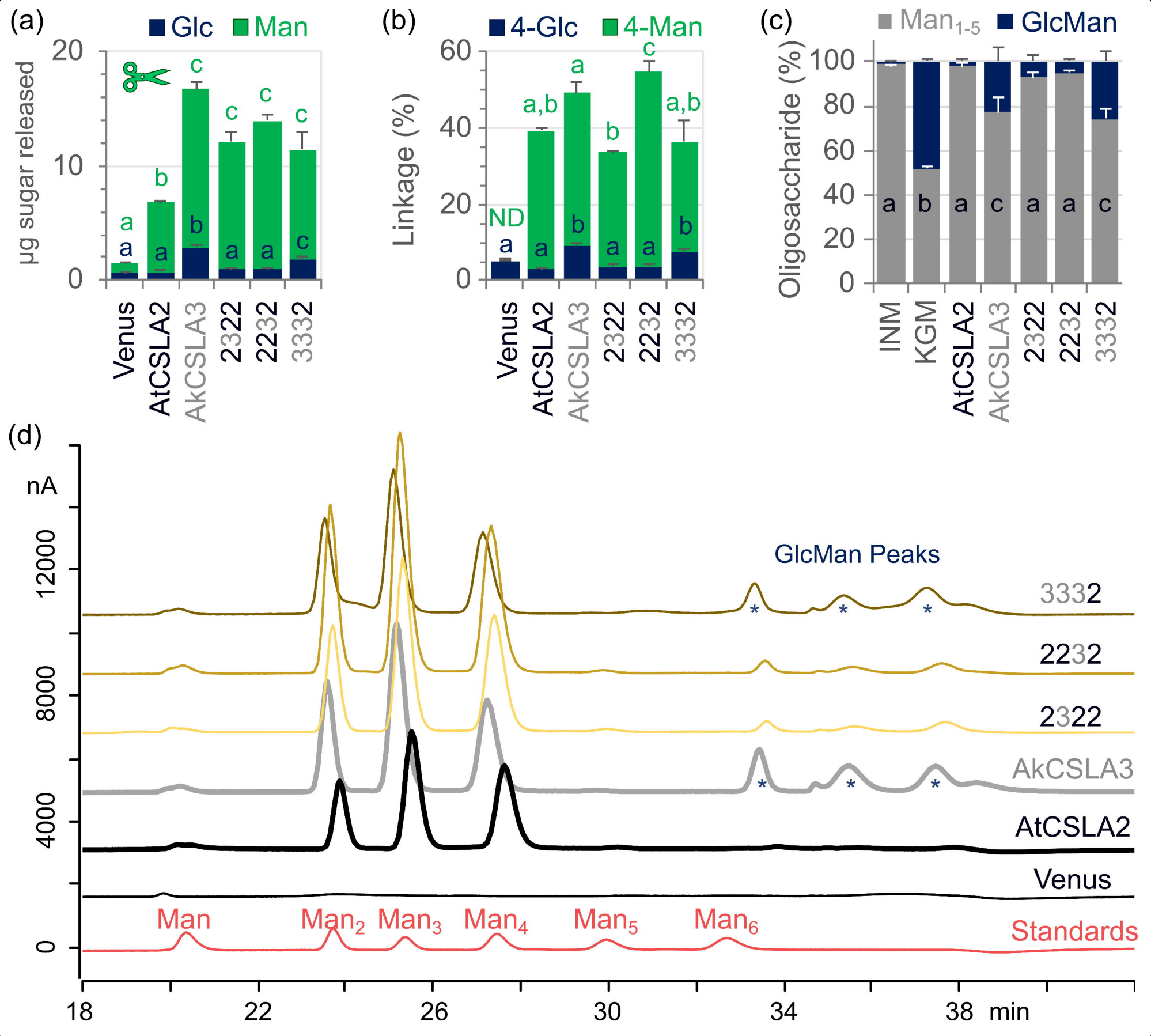
(a)
Glc
Man
µg sugar released
20
10
0
a
a
b
a
c
b
c
a
c
a
c
c
Venus
AtCSLA2
AkCSLA3
2322
2232
3332
(b)
4-Glc
4-Man
Linkage (%)
60
40
20
0
ND
a
a,b
a
a
a,b
b
a
b
a
c
b
Venus
AtCSLA2
AkCSLA3
2322
2232
3332
(c)
Man1-5
GlcMan
Oligosaccharide (%)
100
80
60
40
20
0
a
b
a
c
a
a
c
INM
KGM
AtCSLA2
AkCSLA3
2322
2232
3332
(d)
nA
12000
8000
4000
0
GlcMan Peaks
3332
2232
2322
AkCSLA3
AtCSLA2
Venus
Standards
Man
Man2
Man3
Man4
Man5
Man6
18
22
26
30
34
38
min

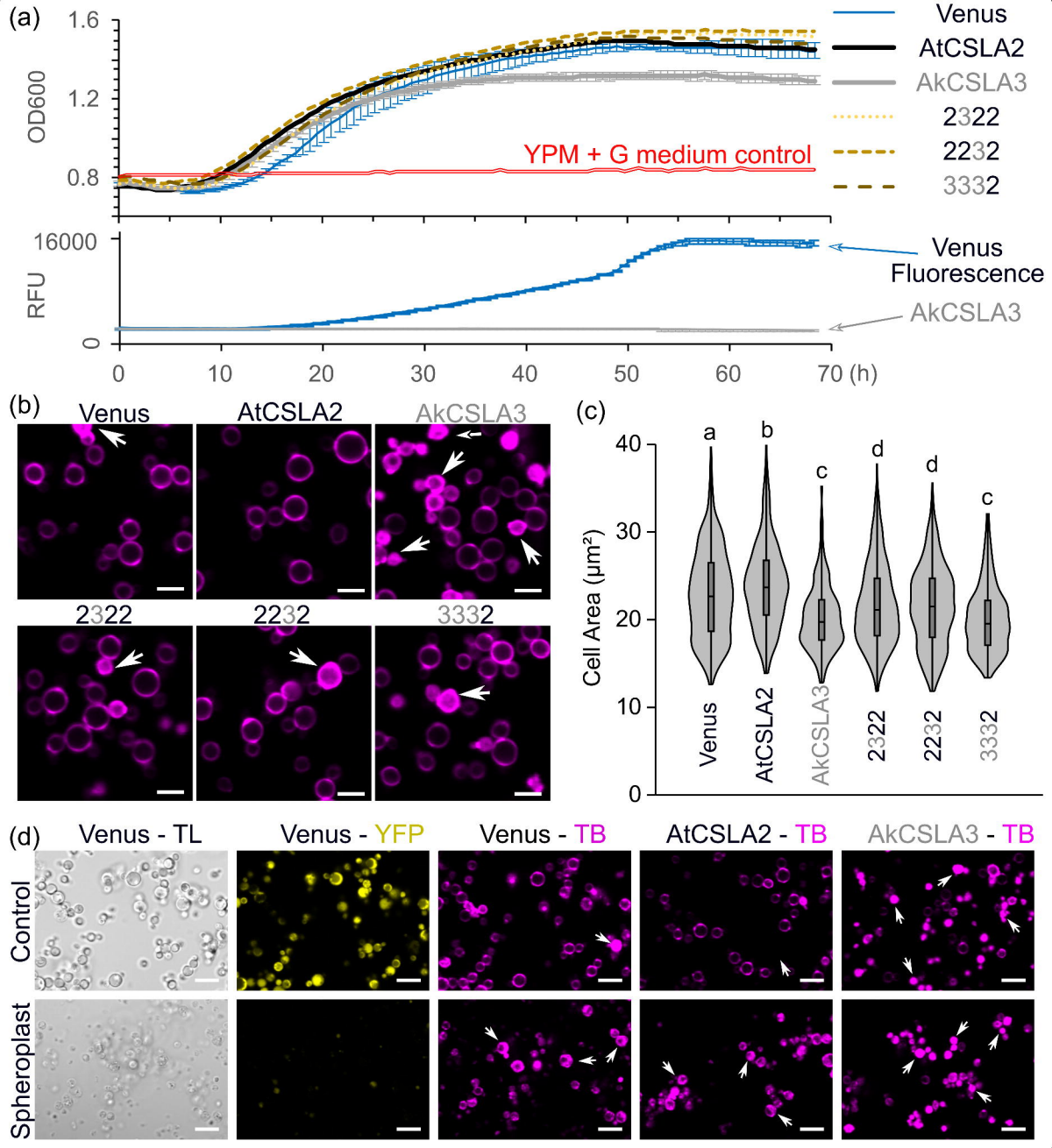
(a)
OD600
1.6
1.2
0.8
YPM + G medium control
Venus
AtCSLA2
AkCSLA3
2322
2232
3332
16000
RFU
0
Venus Fluorescence
AkCSLA3
0
10
20
30
40
50
60
70 (h)
(b)
Venus
AtCSLA2
AkCSLA3
2322
2232
3332
(c)
Cell Area (μm²)
40
30
20
10
0
a
b
c
d
d
c
Venus
AtCSLA2
AkCSLA3
2322
2232
3332
(d)
Venus - TL
Venus - YFP
Venus - TB
AtCSLA2 - TB
AkCSLA3 - TB
Control
Spheroplast